Cronfa - Swansea University Open Access Repository

_____

This is an author produced version of a paper published in:
Nanotechnology

_____

Cronfa URL for this paper:

_____

Paper:

_____

http://www.swansea.ac.uk/library/researchsupport/ris-support/

PAPER • OPEN ACCESS

A proximal retarding field analyzer for scanning probe energy loss spectroscopy

To cite this article: Karl Bauer *et al* 2017 *Nanotechnology* **28** 105711

View the article online for updates and enhancements.

Related content

- Mapping the plasmon response of Ag nanoislands on graphite at 100 nm resolution with scanning probe energy loss spectroscopy
  Shane Murphy, Karl Bauer, Peter A. Sloan et al.

- Detection Improvement for Electron Energy Spectra for Surface Analysis Using a Field Emission Scanning Tunneling Microscope
  Masato Hirade, Toyoko Arai and Masahiko Tomitori

- Imaging surfaceswith reflected electrons
  F Festy, K Svensson, P Laitenberger et al.

A proximal retarding field analyzer for scanning probe energy loss spectroscopy

Karl Bauer, Shane Murphy and Richard E Palmer

Nanoscale Physics, Chemistry and Engineering Research Laboratory, School of Physics and Astronomy, University of Birmingham, Edgbaston, Birmingham, B15 2TT, United Kingdom

E-mail: r.e.palmer@bham.ac.uk

CrossMark

Abstract

A compact proximal retarding field analyzer for scanning probe energy loss spectroscopy measurements is described. Using the scanning tunneling microscope (STM) tip as a field emission (FE) electron source in conjunction with this analyzer, which is placed at a glancing angle to the surface plane, FE sample current and electron reflectivity imaging may be performed simultaneously. This is demonstrated in measurements of Ag nanostructures prepared on graphite by electron-beam lithography, where a material contrast of 13% is observed, with a lateral resolution of 25 nm, between the silver and graphite in electron reflectivity images. Topological contrast mechanisms such as edge enhancement and shadowing are also observed, giving rise to additional features in the electron reflectivity images. The same instrument configuration has been used to measure electron energy loss spectra on bare graphite, where the zero loss peak, π band plasmon loss peak and secondary electron peaks are observed. Using this simple and compact analyzer an STM, with sufficient open access to the tip-sample junction, may easily be augmented to provide simultaneous elemental and topographic mapping, supplementing STM image measurements with FE sample current and electron reflectivity images, as well as electron energy loss spectroscopy measurements, in the same instrument.

Keywords: scanning tunneling microscope, field emission, backscattered electrons, energy loss spectroscopy, silver nanostructures

(Some figures may appear in colour only in the online journal)

1. Introduction

Scanning tunneling microscopy (STM) has become firmly established as a mature technique for surface characterization since it was first demonstrated more than three decades ago [1]. In that time there have been substantial efforts to develop STM in new directions in order to push the boundaries of the information that can be obtained with this tool. For some time now, researchers have been developing a family of scanning probe techniques based on a predecessor of STM, the *Topografiner* [2]. In this configuration the scanning tip is used as a localized emission source of free electrons with which to probe the sample surface. The field-emission (FE) current measured at the sample may be used to construct an image of the surface topography or, with the addition of a suitable detector, electrons leaving the sample surface can be recorded to perform microscopy [3–10] and spectroscopy [11–32].

Depending on the particular instrument configuration a wealth of information about the sample surface can be obtained. For example, FE and secondary electron images with atomic vertical resolution and a lateral resolution of a few nanometres have been demonstrated on graphite [4] and W(110) [9], respectively. In the former case, images were acquired using the FE current measured at the sample, while in the latter case images were recorded using a secondary electron detector placed near to the sample surface. By using an electron energy analyzer the energy spectrum of the electrons leaving the surface can be resolved into back-scattered, secondary and Auger electron peaks. For example,
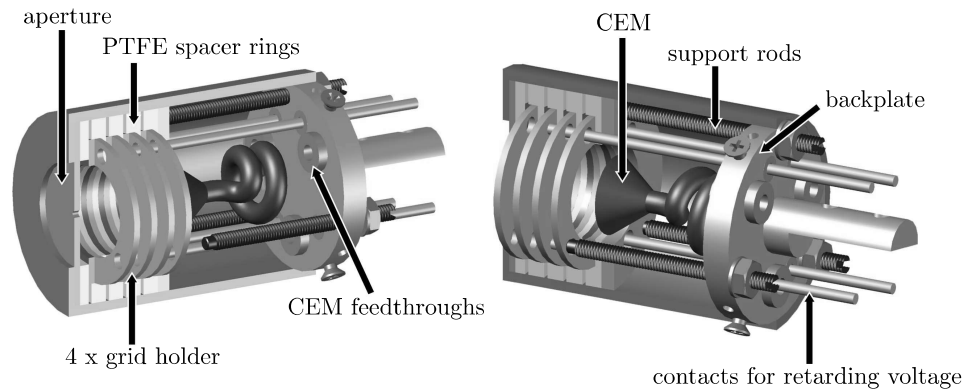
Figure 1. Schematic illustration of the retarding field analyzer. The outer diameter and length of the analyzer are 31 mm and 43 mm, respectively. The entrance aperture, four grid holders, insulating spacer rings, channel electron multiplier (CEM) and backplate with feedthroughs are indicated. The diameter of the grids is 14 mm, while the diameter of the entrance aperture is 3 mm.

scanning probe based Auger electron spectroscopy and energy loss spectroscopy measurements were demonstrated by Reihl and Gimzewski [11] and subsequently by Tomitori *et al* [12] and Eves *et al* [13]. The attraction of combining these experiments in a single STM instrument is that it allows the direct comparison of topograhic information with maps of elemental composition (or electronic excitations such as plasmons) from the same surface area of the sample. For example, Festy and Palmer [21] demonstrated that spectroscopically resolved images of topological features on a roughened Si surface could be obtained with a lateral resolution below 50 nm. More recently, spatially resolved maps of electron energy loss spectra showing clear elemental identification and discrimination were obtained on Ag structures on graphite with a lateral resolution as low as 100 nm [26, 32]. Other noteworthy configurations have produced spin-polarized [33, 34], electron diffraction [35–39] and luminescence [40] measurements.

A key factor for most of these measurements is that the electric field between the tip and sample plays a significant role in the imaging process. Using angle-resolved measurements, Eves *et al* [13] demonstrated that the trajectories of backscattered electrons are deflected back towards the surface by the field between the tip and sample. As a result, the reflected electron signal is sharply peaked in the direction parallel to the surface plane. Therefore, the detector must be placed at a grazing angle to the surface plane in order to maximize the collection of electrons from the surface. One consequence of this is that geometric effects can strongly influence the imaging process and must be considered when evaluating the origins of contrast in the image. Festy *et al* [7] showed that edge enhancement and shadowing effects were important contrast mechanisms in backscattered electron images measured with a retarding field analyzer (RFA) placed at a glancing angle (<5°) to the surface. Another consequence of this configuration is that the high population of backscattered electrons produced in the region directly under the tip apex is suppressed by the electric field and only electrons from an annular region around the tip position are able to reach the detector [15, 16]. Significantly, while this reduces
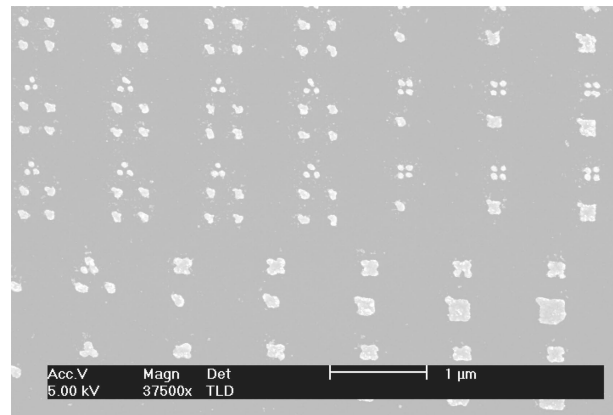

Figure 2. Scanning electron micrographs of 30 nm thick Ag nanostructure array produced on HOPG by electron-beam lithography.

the signal-to-noise ratio it also improves the spatial resolution of the measurements. In these cases, while an unfocused field emitter like a polycrystalline W tip, which is typical for STM measurements, will generate an electron beam with a diameter that is comparable to the tip-sample separation, the measured electron signal will originate from a much smaller area [16]. The size of this probe area depends mainly upon the acceptance angle of the detector and on the field strength and structure (i.e. applied voltage and tip shape), but will generally decrease with emission bias so that high resolution images are best achieved at lower electron energies.

Here, we present a series of scanning probe energy loss spectroscopy (SPELS) measurements obtained using a RFA, an easily implemented and compact device that can be mounted on a standard O.D. 2.75" CF port and can be positioned in close proximity to the sample surface in order to maximize collection efficiency. We demonstrate electron reflectivity measurements of Ag nanostructures on highly oriented pyrolytic graphite (HOPG), which were prepared by e-beam lithography with a minimum structure size of 50 nm. Our measurements show a substructure in the electron reflectivity contrast of the nanostructures, resulting from the
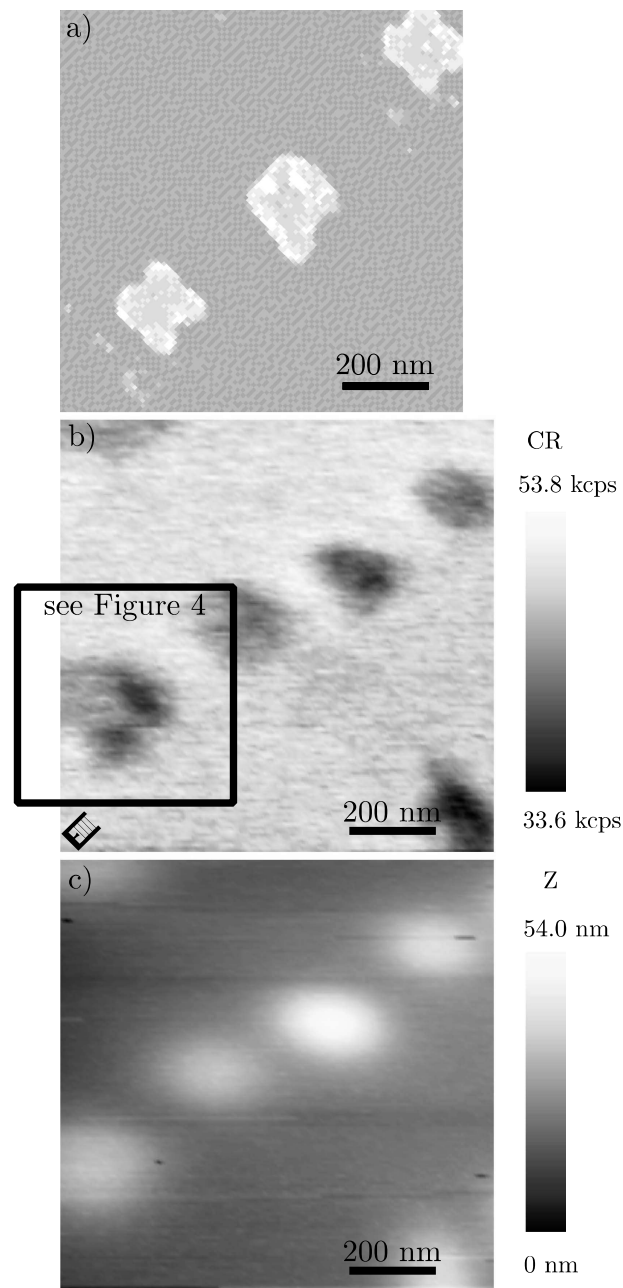
Figure 3. (a) SEM image showing the shape of 30 nm high Ag nanostructures on HOPG. (b) An electron reflectivity image measured of the same type of Ag nanostructures as those shown in (a). (c) The corresponding field-emission image measured with the RFA. These images were taken at a FE voltage of 60 V, a current setpoint of 10 nA and a retarding voltage of 20 V. The tip-sample separation was 100 nm. The orientation of the RFA relative to the scan direction is indicated by the legend in the lower left corner of (b).

interplay between material contrast and topological contrast mechanisms.

2. Experiment

2.1. SPELS instrument

The measurements were performed at room temperature in a modified Omicron STM-1 scanning tunneling microscope, which is housed in an ultrahigh vacuum chamber with a base pressure in the mid 10^{-11} mbar range. To minimize stray electric fields near the sample surface, a grounded Ta foil was added around the STM tip and piezo scanner. The foil can be moved forwards or backwards using a wobblestick in order to facilitate tip exchange. The pre-amplifier near the scan head of the STM-1 was removed and replaced by an amplifier (Femto DLPCA-200) outside the vacuum chamber to allow measurements at higher currents in FE mode using a picoammeter. This instrument has been previously used in combination with a cylindrical sector analyzer with multi-channel detector to map the plasmon response of Ag nanoislands on HOPG with SPELS [32]. For the experiments described here, the analyzer has been replaced with a RFA described below.

Figure 1 shows a schematic of the RFA. It consists of a 1 mm thick stainless steel plate with a 3 mm central aperture, a series of four Au grids (SPI 02199G-AB, bar width 20 μm, hole size 234 μm, 85% open area) for the retarding field and a channel electron multiplier (Photonis CEM 4502) as the detector. Each grid is held between two stainless steel rings that are spot-welded together. A stainless steel rod is welded to each of the four grid holders to act as a contact at the backplate of the analyzer. PTFE distance rings isolate the grid holders from one another and from the grounded casing of the analyzer. The electron multiplier is mounted on a backplate which is fixed to the RFA casing by three screws located at 120° around its circumference. The backplate has seven PTFE-isolated feedthroughs for the four grids and three contacts of the multiplier. Three long screws are used to hold the stack of grids and aperture in place once the backplate is secured to the RFA casing. The RFA is designed to be retractable into a standard O.D. 2.75" CF port during tip and sample exchange. It has an outer diameter of 31 mm, an inner diameter of 14 mm and an overall length of 43 mm. The retarding voltage is applied to the second and third grid, while the first and fourth grids are grounded. The CEM entrance is positively biased at 350 V with respect to the fourth grid to increase detection efficiency at low electron energies. It is operated at space charge saturation while using an Ortec 9302 Amplifier/Discriminator and an Ortec 9349 Ratemeter to count the incident electrons. The distance from the sample to the CEM is 38 mm. This design allows high collection efficiency and can be easily implemented into an existing STM-1 setup.

As backscattered electrons are deflected by the field between the tip and sample, the highest signal can be measured near the sample plane. However, to avoid multiple interference of the electrons with the sample on their way to the detector, we omit the electrons that travel too close to the sample plane by placing the analyzer at a glancing angle of 7° to the sample surface. The distance between the sample and
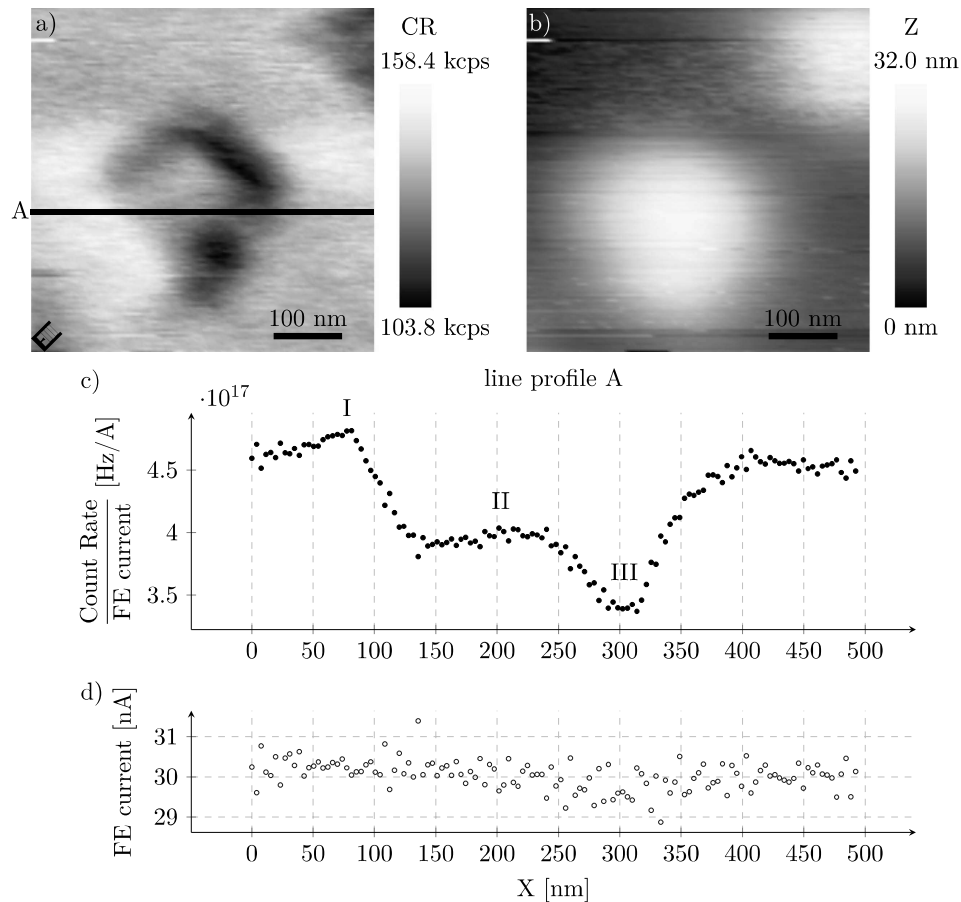
Figure 4. (a) Electron reflectivity image and (b) field emission image of the area marked with the black frame in figure 3. A line-by-line linear correction was applied for both images. The field emission voltage was 55 V, the current setpoint was 30 nA, the retarding voltage was 15 V and the tip-sample separation was 40 nm. The graphs show (c) the count rate per ampere of FE current of the backscattered electrons and (e) the FE current measured along line A in (a). Three distinct regions are visible in the backscattered electron signal, marked I to III, while the field emission current measured at the sample remains constant.

the entrance aperture of the analyzer is 20 mm, which results in a solid angle of 9.2 msr of the 3 mm aperture. The negative FE voltage is applied to the tip while the FE current is measured between the sample and ground. All FE images were obtained in constant current mode. Tungsten tips were prepared using the standard electrochemical etching procedure (i.e. etching in 2 M NaOH with a dc bias of 6 V until drop-off occurs). This was followed *in situ* by prolonged FE at 1–5 μA.

2.2. Electron beam lithography (EBL) of Ag nanostructures

EBL was used to produce well-defined Ag nanostructures on HOPG. SML-100 (EM Resist) was used as the positive tone resist, methyl isobutyl ketone (MIBK) 1:3 diluted in isopropyl alcohol (IPA) as the developer and acetone was used for lift-off. First, 20 μl of SML-100 was spin coated at 500 rpm for 5 s and 3000 rpm for 30 s onto a 12 mm $\times$ 12 mm piece of freshly cleaved HOPG and baked at 160 °C for 3 min on a hotplate. The EBL tool was a Philips XL 30 SEM in combination with an ELPHY Quantum controller (Raith). For the exposure of the structures an electron energy of 3 keV, a

beam current of 40 pA and an area dose of 750 μC cm^{-2} was used. After exposure the samples were developed for 30 s, rinsed in IPA and dried in a nitrogen gas flow. Ag was evaporated at a deposition rate of 2 ML min^{-1} to a thickness of 30 nm. An example of the arrays of different Ag nanostructures produced by electron-beam lithography for these experiments is shown in figure 2.

3. Results and discussion

3.1. Electron reflectivity

Figure 3 shows a series of measurements obtained on some of the Ag nanostructures produced by electron-beam lithography. The shape of the individual nanostructures can be observed in the SEM image shown in figure 3(a). FE measurements were performed on the same type of nanostructures. An example is shown in figure 3(b), which was acquired with a FE voltage of 60 V, a current setpoint of 10 nA and a tip-sample separation of 100 nm. The simultaneously acquired electron reflectivity image of the
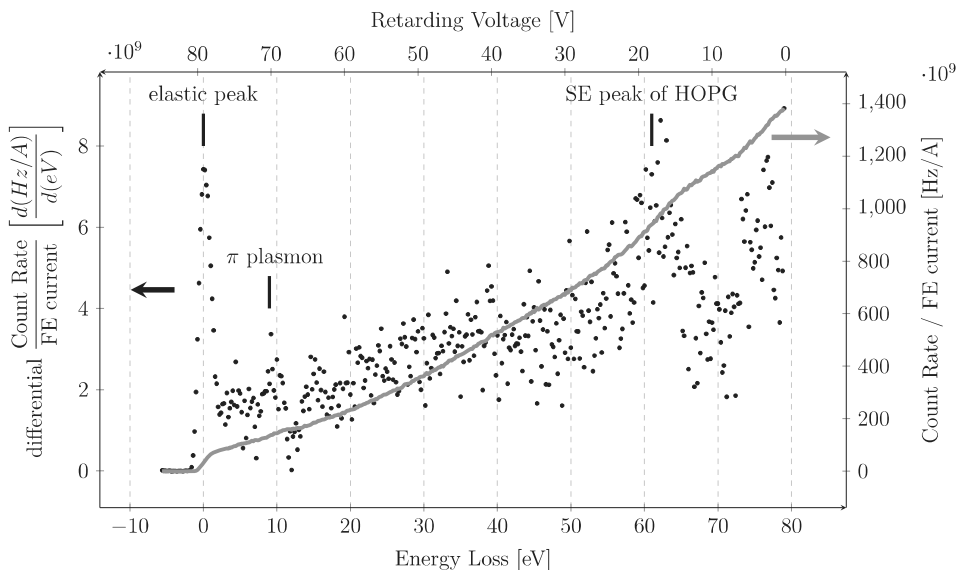
Q1 **Figure 5.** Full electron energy loss spectrum measured on bare HOPG using a field emission voltage of 85 V, a current setpoint of ~175 nA and a 1 mm aperture in the RFA. The solid curve plots the integrated signal measured at the CEM as the retarding voltage is ramped. The scatter plot shows the differentiated signal, which has been smoothed using a moving average filter.

nanostructures is shown in figure 3(c). This was measured with the RFA using a retarding voltage of 20 V to suppress the secondary electron signal so that only the backscattered electron signal is detected. The lateral resolution of the FE in figure 3(b) is limited by the full width of the electron beam, which is comparable to the tip-sample separation of 100 nm. In this case, the FE parameters used have been chosen to obtain a sizeable backscattered electron signal at the RFA (~10^6 counts per second). Higher resolution FE images can be obtained by lowering the FE bias and reducing the tip-sample separation. However, this would result in a substantial reduction in the backscattered electron signal measured by the RFA. The increased spatial resolution observed in the electron reflectivity image in figure 3(c) is due to the fact that the backscattered electrons are detected from a small segment of the annular surface region around the tip, which itself originates from the suppression effect of the tip-sample electric field as described above [15, 16, 41]. Also, as the electron mean free path in a solid is at its minimum at between 50 and 100 eV, the electrons are backscattered from the first few layers of the sample. This leads to a high surface sensitivity of the backscattered electron signal compared to electron imaging techniques operating at higher beam energies.

Another noteworthy point is that the Ag nanostructures yield a lower backscattered electron signal than the surrounding HOPG substrate. We have recently reported on this effect in [32], which is counterintuitive as one would expect a larger electron backscattering cross-section for the element with the higher atomic number. Moreover, since the RFA was configured to suppress the secondary electron signal in these measurements, it is unlikely that variations in the work function of the surface are causing the material contrast. We can only speculate at this point until further experiments are carried out. However, it is possible that differences in electron

diffraction (known to occur in these type of experiments [35–39]) from the Ag nanostructures and the HOPG substrate impact upon how much of the backscattered electron signal is collected by the analyzer from each material. The back-scattered electron images shown here have been obtained with the detector positioned in the lower left corner of the image as indicated by the legend in figure 3(b). On closer inspection of figure 3(b) it is clear that in addition to the material contrast between Ag and graphite, there is also increased reflectivity on areas of the nanostructures that face towards the detector and decreased reflectivity from the edges that face away from the detector. As the electron detector is positioned at a glancing angle to the sample surface high aspect features can block outgoing electrons leading to a lower signal from shadowed regions, while there is less suppression from surfaces that are facing towards the detector.

The various contrast mechanisms are more easily discerned in figure 4, which shows a single Ag nanostructure under high magnification. Figure 4 was taken at a FE voltage of 55 V and a current setpoint of 30 nA, using a retarding voltage of 15 V and a tip-sample separation of 40 nm. Figure 4(c) shows the backscattered electron signal normalized by the FE current, while figure 4(d) displays the FE current, which remains constant due to the feedback control of the tip. A linear fit has been subtracted from each line in figures 4(a) and 4(b) while the data of the graphs has not been processed. The line-profile A in figure 4(c) shows three different regions in the reflectivity image; the area facing the detector (I), the surface of the Ag nanostructure, which has a reduced reflectivity compared to the surrounding HOPG (II) and the surface area where backscattered electrons are blocked from the RFA by the nanostructure (III). The count rate increases at the sides of the nanostructure that face the detector (region I), while the FE current remains constant. The
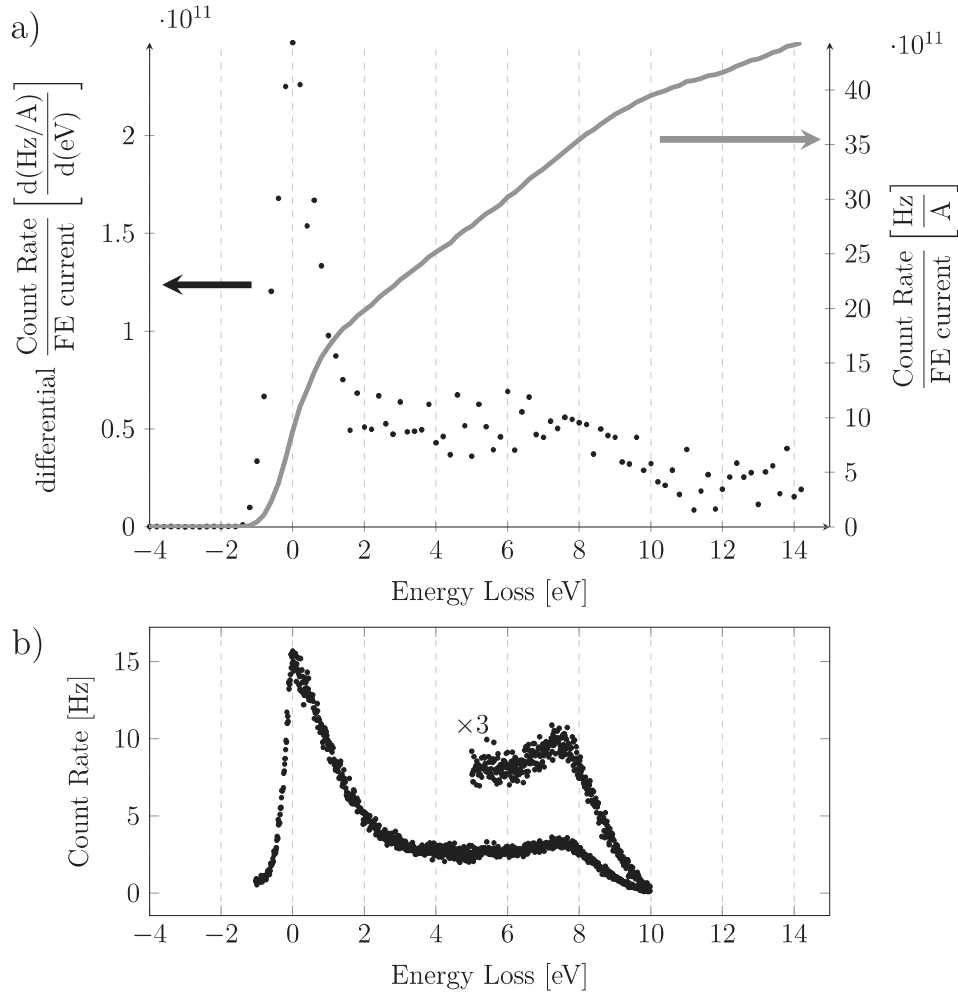
Figure 6. (a) Electron energy loss spectrum measured near the zero loss peak, using a FE voltage of 100 V, a current setpoint of ∼85 nA and a 3 mm aperture in the RFA. The solid curve plots the integrated signal measured at the CEM as the retarding voltage is ramped, while the scatter plot shows the differentiated signal, which has been smoothed using a moving average filter. The full width at half maximum of the zero loss peak is 1.4 eV. (b) For comparison an energy loss spectrum of bare HOPG measured with the cylindrical sector analyzer and multichannel detector described by Murphy *et al* [32].

reflectivity in region II is reduced by 12.6 ± 1.4%, while the drop in region III is 25.3 ± 1.0%. These values and errors have been calculated using linear fits to the count rate measured on the HOPG substrate and Ag island. This substructure is consistent with measurements of other Ag islands. It can therefore be ruled out that the drop in region III is due to a patch of residual resist as these should be distributed arbitrarily on the sample.

The lateral resolution of the electron reflectivity image is taken to be the half-width of the transition from regions II to III, which is 25 nm when measured perpendicular to the Ag island edge.

3.2. Electron energy loss spectra

To investigate the performance of the RFA for SPELS measurements, electron energy loss spectra were measured on bare HOPG. The RFA has been tested with entrance apertures of 1 and 3 mm using the CEM in pulse counting mode. The

aperture size is a trade off between signal and energy resolution, with a smaller aperture giving better resolution at the cost of lower signal. Appropriate aperture sizes have been derived from electron trajectory simulations using the program SIMION. Figure 5 shows the full energy loss spectrum obtained on bare HOPG using a FE voltage of 85 V, a current of ∼175 nA and a 1 mm aperture in the RFA. The solid curve plots the integrated signal measured at the CEM as the retarding voltage is ramped, while the scatter plot shows the differentiated signal, which has also been smoothed using a moving average filter. As the RFA is a high pass filter all electrons with sufficient energy to overcome the retarding potential are detected. Thus, it is difficult to detect plasmon loss peaks against the background of the much larger zero loss peak in the integrated signal measured by the CEM. However, secondary electron peaks in the low kinetic energy range are readily observed as they have comparable intensities to the zero loss peak. These can be seen in figure 5 at

retarding potentials of 19 V and 2 V and agree well with previous SPELS measurements of secondary electron emission spectra of graphite, which were obtained with a concentric hemispherical analyzer [23, 27]. The full width at half maximum of the zero loss peak is around 1.7 eV. Figure 6 compares the energy loss spectrum measured on bare HOPG obtained with the RFA (using a 3 mm aperture) with one measured using a cylindrical sector analyzer used in an earlier study [32]. It is possible to discern a loss peak associated with the graphite π band plasmon at ~ 8 eV [16]. However, given the poor signal-to-noise ratio in the region between the zero loss peak and the π band plasmon loss peak, it has not currently been possible to detect the plasmon loss peak for Ag, which occurs at ~ 3.7 eV [32]. By modulating the retarding field with an ac component and using lock-in detection it might be possible to resolve the Ag plasmon using this RFA in future experiments.

4. Conclusion

A compact and easily implemented proximal RFA for SPELS measurements in a commercial STM has been demonstrated. When positioned close to the sample surface at a glancing angle and used in conjunction with field emitted electrons from the STM tip, material contrast with a resolution of 25 nm can be routinely observed in electron reflectivity images of Ag nanostructures produced by EBL on HOPG. In addition to the material contrast, topological contrast effects such as edge enhancement and shadowing have also been observed. The material contrast resulted in the backscattered electron signal decreasing by about 13% over the Ag nanostructures compared to the surrounding HOPG substrate, which is roughly half of the drop in signal measured in shadowed regions. By sweeping the retarding potential, electron energy loss spectra were measured on bare HOPG where the zero loss, π band plasmon loss peak and secondary electron peaks could be observed. With this analyzer an STM may be easily configured for comprehensive sample characterization as material contrast and topographic information can be obtained simultaneously from electron reflectivity and FE images, and supplemented by electron energy loss spectra and STM measurements using the same instrument.

References

[1] Binnig G, Rohrer H, Gerber C and Weibel E 1982 Surface studies by scanning tunneling microscopy *Phys. Rev. Lett.* **49** 57

[2] Young R, Ward J and Scire F 1972 The Topografiner: an instrument for measuring surface microtopography *Rev. Sci. Instrum.* **43** 999

[3] Fink H W 1988 Point sources for ions and electrons *Phys. Scr.* **38** 260

[4] Sáenz J J and García R 1994 Near field emission scanning tunneling microscopy *Appl. Phys. Lett.* **65** 3022

[5] Frolov V D, Karabutov A V, Konov V I, Pimenov S M and Prokhorov A M 1999 Scanning tunnelling microscopy: application to field electron emission studies *J. Phys. D: Appl. Phys.* **32** 815

[6] Frolov V D, Karabutov A V, Pimenov S M, Obraztsova E D and Konov V I 1999 Application of scanning tunneling-field emission microscopy for investigations of field electron emission from nanoscale diamond films *Ultramicroscopy* **79** 209

[7] Festy F, Svensson K, Laitenberger P and Palmer R E 2001 Imaging surfaces with reflected electrons from a field emission scanning tunnelling microscope: image contrast mechanisms *J. Phys. D: Appl. Phys.* **34** 1849

[8] Kirk T L, Ramsperger U and Pescia D 2009 Near field emission scanning electron microscopy *J. Vac. Sci. Technol. B* **27** 152

[9] Kirk T L, De Pietro L G, Pescia D and Ramsperger U 2009 Electron beam confinement and image contrast mechanism in near field emission scanning electron microscopy *Ultramicroscopy* **109** 463

[10] Kirk T L, Scholder O, De Pietro L G, Ramsperger U and Pescia D 2009 Evidence of nonplanar field emission via secondary electron detection in near field emission scanning electron microscopy *Appl. Phys. Lett.* **94** 153502

[11] Reihl B and Gimzewski J K 1987 Field emission scanning Auger microscope (FESAM) *Surf. Sci.* **189/190** 36

[12] Tomitori M, Terai H and Arai T 1999 Energy spectrum of backscattered electrons excited by a field emission scanning tunneling microscope with a build-up [111]-oriented W tip *Appl. Surf. Sci.* **144–145** 123

[13] Eves B J, Festy F, Svensson K and Palmer R E 2000 Scanning probe energy loss spectroscopy: angular resolved measurements on silicon and graphite surfaces *Appl. Phys. Lett.* **77** 4223

[14] Tomitori M, Hirade M, Suganuma Y and Arai T 2001 An applicability of scanning tunneling microscopy for surface electron spectroscopy *Surf. Sci.* **493** 49

[15] Palmer R E 2002 New directions in nanoscience: new challenges for surface analysis *Surf. Interface Anal.* **34** 3

[16] Palmer R E, Eves B J, Festy F and Svensson K 2002 Scanning probe energy loss spectroscopy *Surf. Sci.* **502–503** 224

[17] Miyatake Y, Nagamura T, Hattori K, Kanemitsu Y and Daimon H 2002 Development of electron source for Auger electron spectroscopy in scanning probe microscope systems *Japan. J. Appl. Phys.* **41** 4943

[18] Tomitori M, Hirade M, Suganuma Y and Arai T 2002 Surface spectroscopy utilizing field electron emission from thermal-field treated tips in STM *J. Surf. Anal.* **9** 359

[19] Hirade M, Arai T and Tomitori M 2003 Detection improvement for electron energy spectra for surface analysis using a field emission scanning tunneling microscope *Japan. J. Appl. Phys.* **42** 4837

[20] Miyatake Y, Nagamura T, Hattori K, Kanemitsu Y and Daimon H 2003 Development of scanning probe microscope for Auger analysis *Japan. J. Appl. Phys.* **42** 4848

[21] Festy F and Palmer R E 2004 Scanning probe energy loss spectroscopy below 50 nm resolution *Appl. Phys. Lett.* **85** 5034

[22] Hirade M, Arai T and Tomitori M 2006 Energy spectra of electrons backscattered from sample surfaces with heterostructures using field-emission scanning tunneling microscopy *Japan. J. Appl. Phys.* **45** 2278

[23] Yin J, Pulisciano A and Palmer R E 2006 Local secondary-electron emission spectra via scanning probe energy loss spectroscopy *Small* **2** 744

[24] Zhou X, Xu C K, Wei Z, Liu W J, Li J W, Chen X J, Williams J F and Xu K Z 2008 Angle and energy dispersive multichannel electron energy spectrometer for surface analysis *J. Electron Spectrosc. Relat. Phenom.* **165** 15

[25] Pulisciano A, Park S J and Palmer R E 2008 Surface plasmon excitation of Au and Ag in scanning probe energy loss spectroscopy *Appl. Phys. Lett.* **93** 213109

[26] Xu C K, Chen X J, Zhou X, Wei Z, Liu W J, Li J W, Williams J F and Xu K Z 2009 Spatially resolved scanning probe electron energy spectroscopy for Ag islands on a graphite surface *Rev. Sci. Instrum.* **80** 103705

[27] Lawton J J, Pulisciano A and Palmer R E 2009 Local secondary-electron emission spectra of graphite and gold surfaces obtained using the scanning probe energy loss spectrometer (SPELS) *J. Phys.: Condens. Matter* **21** 474206

[28] Song M Y, Robinson A P G and Palmer R E 2010 Fabrication of co-axial field emitter tips for scanning probe energy loss spectroscopy *Nanotechnology* **21** 155304

[29] Song M Y, Lawton J J, Robinson A P G and Palmer R E 2010 Scanning probe energy loss spectroscopy with microfabricated coaxial tips *Phys. Rev.* B **81** 161411(R)

[30] Xu C K, Zhang P K, Meng L and Chen X J 2014 A double toroidal analyzer for scanning probe electron energy spectrometer *Chin. Phys.* B **23** 073402

[31] Xu C K, Liu W J, Zhang P K, Li M, Zhang H J, Xu K Z, Luo Y and Chen X J 2014 Nonlinear inelastic electron scattering revealed by plasmon-enhanced electron energy-loss spectroscopy *Nat. Phys.* **10** 753

[32] Murphy S, Bauer K, Sloan P A, Lawton J J, Tang L and Palmer R E 2015 Mapping the plasmon response of Ag nanoislands on graphite at 100 nm resolution with scanning probe energy loss spectroscopy *Appl. Phys. Express* **8** 126601

[33] Allenspach R and Bischof A 1989 Spin-polarized secondary electrons from a scanning tunneling microscope in field emission mode *Appl. Phys. Lett.* **54** 587

[34] First P N, Stroscio J A, Pierce D T, Dragoset R A and Celotta R J 1991 A system for the study of magnetic materials and magnetic imaging with the scanning tunneling microscope *J. Vac. Sci. Technol.* B **9** 531

[35] Mizuno S 2001 Development of an advanced low-energy electron diffraction technique using field-emitted electrons from scanning tunneling microscope tips *J. Vac. Sci. Tehnol.* B **19** 1874

[36] Mizuno S, Fukuda J and Tochihara H 2002 Extraction of scattered low-energy electrons in field emission conditions *Surf. Sci.* **514** 291

[37] Mizuno S, Fukuda J, Iwanaga M and Tochihara H 2004 Scattering patterns and energy distribution of scattered electrons under field emission conditions of scanning tunneling microscopy *Japan. J. Appl. Phys.* **43** 5501

[38] Mizuno S, Rahman F and Iwanaga M 2006 Low-energy electron diffraction patterns using field-emitted electrons from tungsten tips *Japan. J. Appl. Phys.* **45** L178

[39] Onoda J, Kanaoka T, Kumon M and Mizuno S 2012 Development of LEED apparatus using nano-tips fabricated by field-assisted etching *e-J. Surf. Sci. Nanotechnol.* **10** 292

[40] Berndt R and Gimzewski J K 1991 Inelastic tunneling excitation of tip-induced plasmon modes on noble-metal surfaces *Phys. Rev. Lett.* **67** 3796

[41] Li M, Xu C K, Zhang P K, Li Z and Chen X J 2016 Electron energy spectroscopy mapping of surface with scanning tunneling microscope *Rev. Sci. Instrum.* **87** 086108